Fusion Engineering and Design 219 (2025) 115298

Contents lists available at ScienceDirect

Fusion Engineering and Design

journal homepage: www.elsevier.com/locate/fusengdes

A laser-based diagnostic for *in situ* monitoring of fuel retention in ITER

A. Huber [a,*], Ph. Andrew [b], G. Sergienko [a], J. Assmann [a], D. Castano [a], A. De Schepper [a], S. Friese [a], I. Ivashov [a], D. Kampf [c], Y. Krasikov [a], H.T. Lambertz [a], Ph. Mertens [d], K. Mlynczak [a], K. Rasinska [a], M. Schrader [a], D. Van Staden [c], A. Terra [a], Xi Jiang [b], M. Zlobinski [a], A. Reutlinger [c], S. Brezinsek [a], Ch. Linsmeier [a]

[a] Institute of Fusion Energy and Nuclear Waste Management–Plasma Physics, Forschungszentrum Jülich GmbH, Germany
[b] ITER Organization, Route de Vinon, CS 90 046, Saint-Paul-lez-Durance 13067, France
[c] KTO Kampf Telescope Optics GmbH, Germany
[d] FUSE-L Fusion Specific Expertise-Liege, Route du Condroz 111B, Liège B-4031, Belgium

ARTICLE INFO

Keywords:
Laser-based diagnostic
ITER
Tritium retention
Plasma wall interaction
LID-QMS
Tungsten

ABSTRACT

This paper addresses the critical challenge of tritium inventory control in ITER and future fusion devices, emphasizing the necessity for precise measurement and spatial distribution of tritium within the vacuum vessel. The proposed laser-based T-monitor diagnostic system from Forschungszentrum Jülich employs Laser-Induced Desorption (LID) combined with Residual Gas Analysis (RGA) to measure hydrogen isotope concentrations on the inner divertor tiles. Key design elements include high-power laser integration, advanced optical systems, and a Fast Scanning Mirror Unit for accurate laser spot positioning. The diagnostic aims to measure *in situ* tritium retention, improving operational safety and efficiency in nuclear fusion environments.

1. Introduction

A central challenge for ITER and future fusion devices is controlling the tritium inventory within the vacuum vessel, which is crucial for facility safety. As a licensed nuclear facility, ITER must limit tritium retention to 1 kg to reduce the risk of potential releases during accidents. This limit includes 120 g in cryopumps and 180 g of measurement uncertainty, allowing a maximum of 700 g within vessel components [1].

The current first wall design still considers beryllium (Be) as the material for the main chamber wall. However, the ITER Organization (IO) has been extensively discussing the potential shift from beryllium (Be) to tungsten (W) as the first wall (FW) material. Although a final decision has not yet been made, the IO initiated a re-baselining exercise in early 2023, with a key component being the transition of the FW material from beryllium to tungsten [2]. The benefits of using tungsten include lower sputtering yield, a higher energy threshold, improved erosion lifetime, a higher melting point, and greater resilience during disruptions. However, this change increases the tungsten plasma-facing surface area, raising the risk of higher core plasma tungsten content, which could lead to radiative losses and challenges in maintaining H-mode. Furthermore, replacing beryllium reduces impurity gettering, particularly for oxygen, which could complicate plasma start-up. To address this, a boronization of the first wall will be implemented, though it may increase tritium (T) fuel retention due to co-deposition.

Full-tungsten devices generally apply a thin boron (B) coating to plasma-facing components (PFCs) through glow discharge plasma-assisted chemical vapor deposition (boronization), which facilitates plasma initiation and start-up. However, in ITER this method poses the risk of increased tritium fuel retention, as the eroded boron may co-deposit with the fuel.

The laser-based T-monitor diagnostic system developed by Forschungszentrum Jülich will remotely measure the tritium content on ITER's inner divertor tiles. This measurement technique relies on laser-induced desorption (LID) and the detection of released gases using a residual gas analyzer (RGA). The method has been successfully demonstrated in laboratory settings [3], as well as in fusion devices like TEXTOR [4,5] and JET [6] In these devices, with low-Z materials in the main chamber, the hydrogen isotope content was primarily built up through wall erosion and the co-deposition of hydrogen isotopes, particularly in magnetically shadowed regions [7] and on the inner tungsten divertor [8]. This phenomenon was also anticipated in the original ITER configuration, where beryllium was used in the main

* Corresponding author.
E-mail address: A.Huber@fz-juelich.de (A. Huber).

https://doi.org/10.1016/j.fusengdes.2025.115298
Received 18 December 2024; Received in revised form 27 May 2025; Accepted 23 June 2025
Available online 29 June 2025

chamber. However, in a fully tungsten ITER, the main sources of tritium retention will shift to the co-deposition of hydrogen isotopes with eroded and re-deposited boron (B) and tungsten (W), alongside implantation into the tungsten material [2]. As boron is eroded, it is expected to migrate and deposit at the divertor [9]. The phenomenology is similar to that of beryllium (Be) eroded from the first wall, although it is quantitatively different for boron since the source can be more accurately quantified (i.e., the boron introduced by boronization, while Be is produced by erosion of the wall) [10]. As mentioned above, the B coating in a fully W machine replaces the oxygen-gettering role of Be by boronization, although the coating is relatively short-lived.

This article introduces an optical and mechanical design with a high-power laser and metallic mirrors for efficient NIR beam transport and coaxial VIS/NIR observation. The mirrors, made from durable, non-standard substrates, are designed to meet the unique demands of ITER's nuclear environment, with attention to detection limits and T-Monitor diagnostic requirements.

2. The method and measurement requirements

The core concept of laser-based LID-QMS diagnostics is to heat specific areas of the first wall using intense laser radiation between plasma discharges under vacuum conditions. The peak temperatures must be sufficient to desorb the entire amount of hydrogen isotopes and their compounds from the surface layer in a single laser pulse. Wall particles, including atoms, molecules, and clusters, are released through desorption and detected by Residual Gas Analysis. A detailed description of the RGA system intended for use on ITER can be found in [11], it is beyond the scope of this paper. The technique enables the measurement of thermally released gases at different locations, providing spatially resolved data. The spatial resolution of T content measurements on ITER requires two measurement points in the poloidal direction on the same poloidal monoblock and at least six measurement points in the toroidal direction on the same toroidal monoblock. Given that a divertor monoblock measures 10 mm by 30 mm (poloidal/toroidal directions) [12], the laser spot size should be 5 mm in diameter or smaller.

The power density and pulse duration must be sufficiently high to heat the surface to 1600 K, the temperature at which, based on our experience, all hydrogen isotopes are fully desorbed from the expected deposited layer. This temperature of 1600 K is adequate to desorb the entire hydrogen isotope content from both Be:D and B:D deposition layers [3–6]. It is worth mentioning that the first laser desorption experiments were conducted in TEXTOR on B:D deposited layers [4]. In these experiments, the D content of the B:D layer was completely released from a laser spot with an area of approximately 0.4 cm^2 using a laser pulse of 0.3 ms duration and 5 J of pulse energy. This corresponds to a maximum absorbed power density of about 415 MW/m^2. On the other hand, thermal heating must remain below the melting point of bulk tungsten ($T_{W\_melting} = 3695$ K) to prevent significant sublimation of the tungsten material. To achieve a surface temperature of 1600 K on a 5 mm spot, the required absorbed power density is approximately 665 MW/m^2 for a 1 ms pulse and about 380 MW/m^2 for a 3 ms pulse. These estimates are based on a simplified model that accounts for finite heat penetration depths, using the infinite half-space approximation to estimate the laser heat propagation. The calculations were performed for tungsten, considering the laser absorption power fraction of 0.5, as measured in the laboratory on tungsten samples at the NIR laser wavelength $\lambda = 1.07$ μm. The special case involves measurements in the erosion zone on pure W material without deposited layers. TMAP-7 modeling [13] shows that, using a longer exposure duration of 10 ms, the simulation predicts that approximately 80% of the D is released at a surface temperature of 1000 K. The fraction of released D is expected to depend on the steady-state exposure temperature of W during D implantation, and this will be the subject of future work. It should be noted that if a single pulse is not sufficient to desorb the entire fuel content in this case, a multiple-pulse solution should be considered. Retention in the erosion zone of pure tungsten could be affected by neutron irradiation. The effect of neutron irradiation depends strongly on the level of irradiation damage, expressed in terms of displacements per atom (dpa). At ITER's end-of-life, the maximum damage values are estimated to be 0.54 dpa on tungsten at the inner divertor target [14]. As reported in [15], retention is generally found to increase with the presence of displacement damage. It was found [15,16] that at a damage dose of 0.23 dpa, a maximum deuterium concentration of about 1.4 at% is reached. This is much lower than the fuel concentration expected in the boron layer. Nevertheless, the measurements with the T-monitor diagnostic in the erosion zone of pure tungsten are foreseen.

A key requirement for the T-monitor diagnostic is the ability to measure the surface tritium concentration at $n_{surf} = 2.1 \times 10^{21}$ T atoms/m^2, with a required relative accuracy of 20% [17]. The measurements shall be conducted on the inner divertor baffle. These requirements remain the same regardless of the first wall material configuration. The measurements of the T-inventory, combined with codes like Monte-Carlo code ERO2.0 [18] or WallDYN [19], will provide the tritium inventory content inside the vacuum vessel.

This target concentration is expected to be achieved in the configuration with beryllium in the main chamber, with a tritium inventory of 10 g in the vacuum vessel (VV). This amount is expected after approximately 25 plasma pulses (each lasting 400 s with $Q_{DT} = 10$), with a deposition rate of about 0.4 g per full-power pulse [20].

For the full-W device, the primary sources of tritium retention will be co-deposition with eroded and re-deposited boron and tungsten, as well as implantation in tungsten. In terms of boron co-deposits, migration simulations are detailed in Section 4.2 of paper [2]. To ensure conservative tritium retention estimates for ITER, a fixed value of $\{H/D/T\}/B = 0.5$ is assumed. Boron co-deposits can retain a maximum of 4, 8, and 12 g of H, D, and T, respectively, per 50 nm of boronization on ITER, depositing 86 g of boron (see Section 4.2 in [2]). Applying these estimates, the total tritium retention in boron co-deposits is estimated to be between 320 and 380 g by the end of the DT-1 phase, with the variance due to different choices that may be made during the execution of the FPO-4 and 5 campaigns [2].

The selection of laser pulse duration is critical for ensuring the required accuracy of T-inventory measurements. Fig. 1a illustrates the

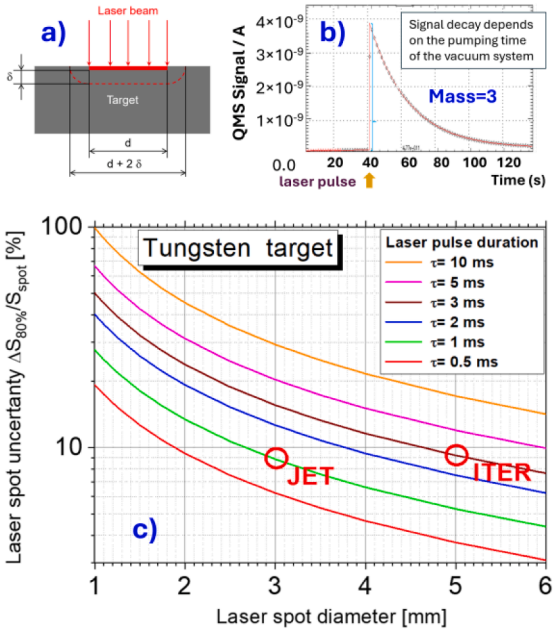

Fig. 1. a) Impact of lateral heat propagation on the heated area, b) RGA signal during laser illumination, c) Dependence of the uncertainty of the spot area on the laser spot size for different laser pulse durations.

impact of lateral heat propagation on the heated area. Due to the finite laser exposure time, the spot diameter becomes $d + 2\delta$, where d is the designed laser spot diameter, and δ represents the increase in diameter caused by lateral heat propagation, which becomes larger with a longer laser pulse duration. In general, the pulse duration should be minimized to reduce the impact of lateral heat propagation on the desorption area. However, the heat penetration depth must be sufficient to desorb fuel from the deposited layer, which is expected to be around 100 μm for a beryllium material configuration in ITER [1]. For a full-W configuration, the expected depth is smaller [2]. The laser parameters, determined considering a maximum coating layer thickness of 100 μm, are valid for both material configurations, making the diagnostic method universally applicable. Fig. 1c illustrates the operational parameter space for the laser, represented in terms of spot diameter and uncertainty for different pulse durations. The uncertainty is defined as $\Delta S/S = (S_h - S)/S$, where S is the laser spot area and S_h is the heated area, including the lateral heat propagation, where the temperature T is above 80% of the maximum temperature in the illuminated spot (Fig. 1a).

As shown, for ITER, a 5 mm laser spot and pulse durations between 1 ms and 3 ms are needed to maintain less than 10% measurement uncertainty, with ≈5 mm spatial resolution required for single-point measurements.

Additionally, Fig. 1b shows an example of the RGA signal (partial pressure of mass 3, which corresponds to the HD molecules) during laser illumination of the investigated samples in the lab. The laser illumination triggers an abrupt jump (Δp) in the pressure signal, followed by an exponential decay, the time constant of which depends on the pumping speed. From the Δp, the number of released HD molecules can be evaluated. More details about the evaluation procedure can be found, for example, in [4]. The measurement requirements for the T-monitor diagnostic are as follows: the diagnostic should provide measurements of protium (H), deuterium (D), and tritium (T) concentration at the inner baffle, where co-deposits are primarily expected to form. The scanning area extends ≈0.54 m in the poloidal direction and ≈0.11 m in the toroidal direction as shown in Fig. 2. Please note that the toroidal extension should include three monoblocks: two monoblocks are located in the deposition zone, and one is in the erosion zone. The measurements must be taken under good vacuum conditions and when the plasma operation is not active. The expected tritium areal density is between 10^{21} and $2 \times 10^{24} m^{-2}$.

3. Optical design and mechanical layout

The optical components, consisting of both in-vessel and ex-vessel components, are distributed across various areas (see Fig. 3a). The in-vessel components, located within the port inside the Diagnostic Shielding Module (DSM) [21], perform re-imaging of the Intermediate Focus Image 2 on to the divertor surface. Ex-vessel components are positioned in the Interspace Support Structure (ISS) area, within the bioshield, in the Port Cell Support Structure (PCSS), and in the Tritium building. These groups of optical components do not have a stable common platform, which can lead to misalignment between groups during operation due to thermal expansion of the optical components' supporting structures.

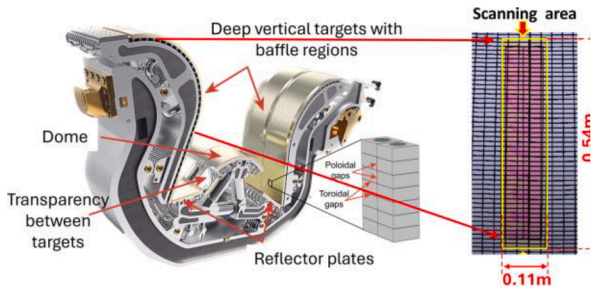

Fig. 2. A single ITER tungsten (W) divertor cassette, highlighting the scanning area on the inner divertor baffle.

The Fast Scanning Mirror Unit (FSMU) in the ISS, along with the optical dog-leg within the bioshield, is crucial for aligning the optical system. The FSMU performs 1:1 re-imaging of the Intermediate Focus Image 1 at the PCSS on to the Intermediate Focus Image 2 in the port plug and can be also used to correct the misalignment. Alignment checks and corrections will occur before each measurement. Space limitations restrict the sizes of optical components, and the extended distances impact optical resolution due to diffraction limits. Since the illuminated surface needs to be examined, the same optical system is used for both launching the high-power laser and collecting the return light for analysis by one of the three integrated instruments. This co-axial configuration supports three instruments covering different wavelength ranges: visible (VIS) camera, near-infrared (NIR) camera, and a 3-pyrometer optical setup.

In Fig. 3a, an overview of the complete beam path is presented, starting from the laser fibre exit (laser injection) at right. The optical system can be simply described as a pupil that follows an image or focus, as illustrated in Fig. 3. Two focal planes are predefined: the laser fibre cross-section and the laser spot at the divertor, which serves as the image of the laser fibre. Laser-fibre diameter is 300 μm and the required laser spot size at the target is 5 mm in diameter. The entrance pupil of the optical system is defined by the image of the laser beam at the steering mirror M7 (≈ 56 mm) and is located inside the first wall. An intermediate focal plane should be positioned inside the DSM between two mirrors, maximizing the distance between them to increase the laser beam diameter on the mirrors, thereby reducing the laser power density on the reflecting surface and minimizing the risk of damage. Since a toroidal mirror will be used due to tolerances in the DSM, this imaging mirror must be M3, resulting in an intermediate image formed between M4 and M5. Furthermore, the image size for full illumination of the scanning area at the vacuum window (VW) must be smaller than 160 mm (the clear aperture of the VW). The DSM intermediate image is reimaged after the dog-leg near the bio-shield. Reimaging the "Intermediate Focus Image 1″ guides the beams to the focal planes of VIS channel, NIR channel and pyrometer as well as to the laser fibre.

Fig. 4 shows the spot diagrams for the central line of sight with the Airy disks for comparison. It illustrates the distribution of light points (spots) at the divertor baffle (image plane) for given field points at the laser fibre input, showing how accurately the system can focus and whether there are optical aberrations. The Airy disk represents the smallest achievable spot size due to diffraction and, in this case, has a radius of approximately 140 μm. The spot diagram sizes are smaller than the Airy disks; therefore, the optical system is called diffraction-limited.

The diffraction-limited resolution of the optical system is influenced by the laser wavelength λ and entrance pupil diameter *D*, as described by the formula $\Delta x = (1.22\ \lambda / D)\ L$, where *L* is the distance to the target. In this design, the $D = 56$ mm diameter entrance pupil, located at $L = 5.2$ m from the divertor target, results in a laser spot size uncertainty of about $\Delta x = 0.12$ mm at a wavelength of $\lambda = 1.07$ μm.

3.1. In-vessel optics

The in-vessel optics consists of six mirrors, along with the vacuum window, which includes two tilted uncoated fused-silica discs each having a thickness of 17 mm, as illustrated in Fig. 5: a) the side view, b) the top view of the optical design, and c) the in-vessel mirror assemblies with the pneumatic shutter system. The design was developed in accordance with the requirement for an optical dogleg inside the port plug, ensuring that the neutron streaming is reduced. Only metal mirrors are used in the optics within the port plug. A viewing path through the diagnostic first wall allows observation of the inner divertor baffle. The optical and shutter components typically operate in the range of 100–240 °C. Optical system will operate in both forward and backward

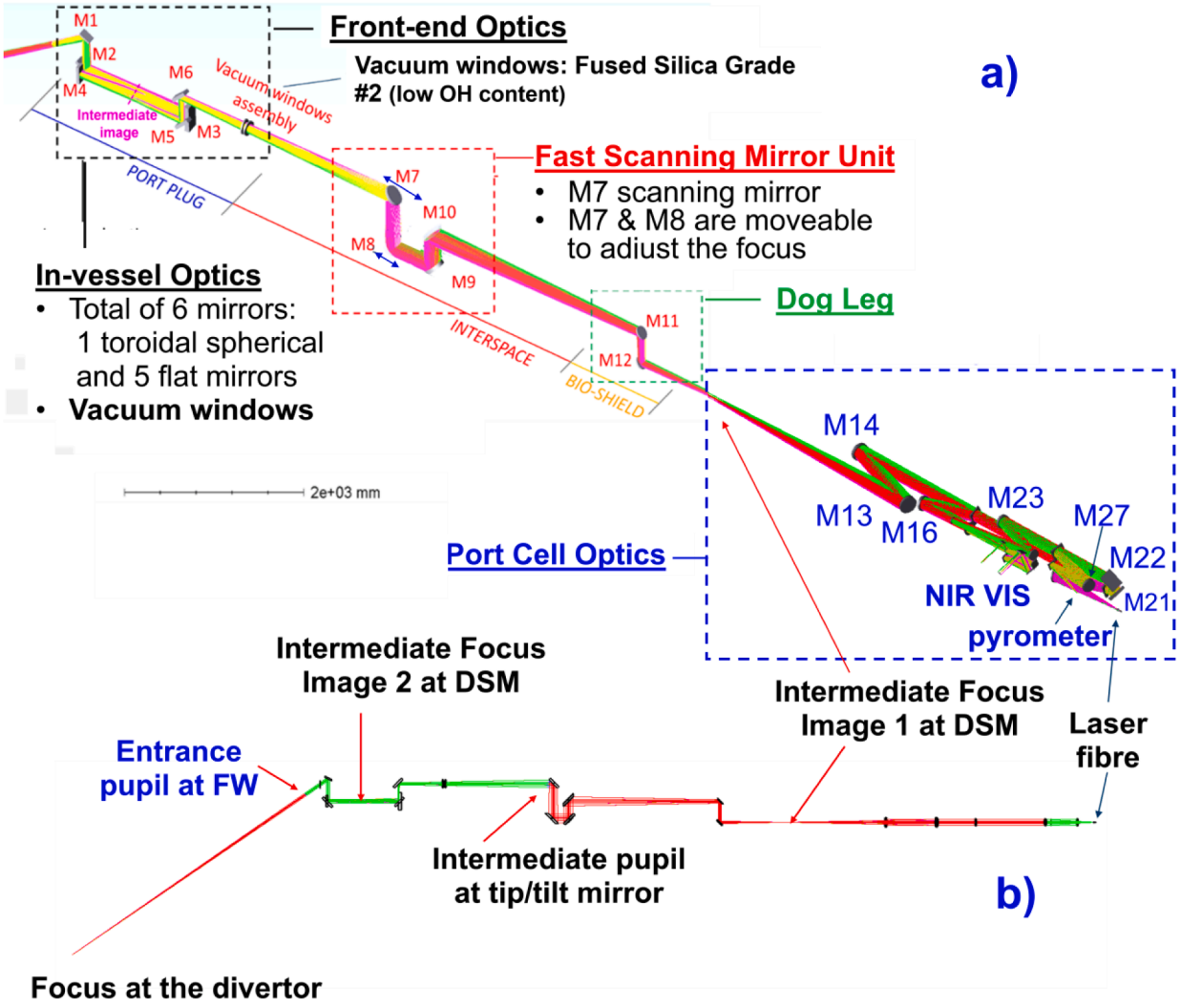

Fig. 3. Overview of the optical layout of the T-Monitor diagnostic system: a) entire optical system; b) Optics for laser beam transport.

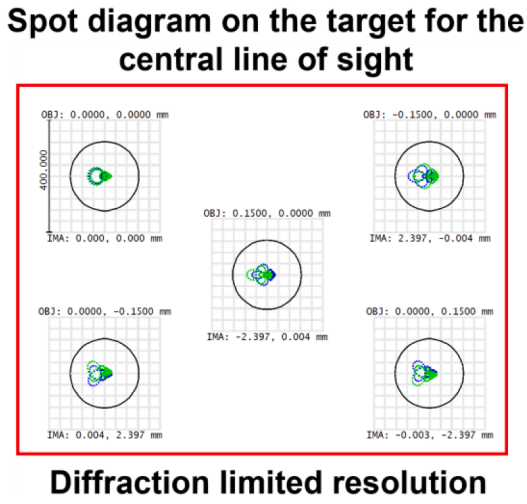

Fig. 4. Spot diagram on the target for the central line of sight with the Airy disks for comparison.

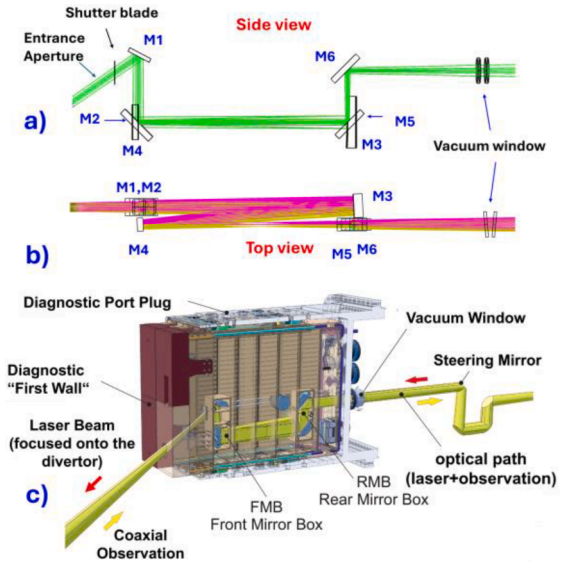

Fig. 5. In vessel optics and shutter a) optical design side view b) optical design top view c) the mechanical layout.

directions. All optical elements are flat, except for M3, which has a toroidal shape. The spacing between the optics is large enough in order to cope with the thermo-mechanical deformations, as the mirrors M1 to

M6 are combined in two separate subassemblies: front mirror box (FMB) for M1, M2 and M4 and rear mirror box (RMB) for M3, M5 and M6 as shown in Fig. 6a. To verify the optical performance, a thermal-mechanical simulation was conducted in ANSYS, considering system assembly, plasma operations, and the Tritium monitor laser scanning. The distorted mirror surfaces from this simulation were analyzed using ray-tracing in Zemax [22]. Ref. [23] focused on the specific topic of the impact of powerful laser exposure on the mirror surface in different operation modes, with varying numbers of laser pulses. The analysis reported in this paper shows that the system's optical performance criteria meet acceptable limits for spot defocusing and positional shift.

Additionally, the diagnostic system includes a pneumatic shutter inside the port plug (Fig. 6b) to protect M1 against deposition and erosion, especially during cleaning discharges or by fast neutral particles during plasma operation. This shutter system consists of a linear actuator, a cooled shutter blade, and arms. The pneumatic design ensures high reliability and friction-free operation. The shutter operates with a 30 mm piston stroke, requiring 500 N of force to open, and has an arm stiffness of about 18 N/mm. Both the shutter and the front mirror box are cooled by water, and the shutter actuator uses pressurized helium (up to 1.2 bar). The shutter blade also monitors optical transmittance at a laser wavelength of 1.07 μm, with a rear surface designed as a calibration source that can be heated to 1200 °C. More details about the usage of the shutter blade as a calibration source can be found in [24]. Since Ref. [24] is dedicated specifically to the calibration topic, the present paper will not discuss the calibration issue in detail.

3.2. Ex-vessel optics

3.2.1. Fast scanning mirror unit in the ISS area

The T-monitor diagnostic is designed to measure the T content across the specified spatial range. For precise laser positioning onto the divertor baffle, the T-monitor's Fast Scanning Mirror Unit is a device developed within the diagnostic system to enable rapid (up to 60 Hz) and accurate mirror steering. The FSMU contains four mirrors and operates as an optical relay between Intermediate Focus Image 1 and Intermediate Focus Image 2.

The M7 beam-pointing mirror provides six degrees of freedom, allowing vertical tip/tilt angles of ±0.6° and horizontal angles of ±0.16° To account for a 10 mm oversizing of the in-vessel mirrors and alignment tolerances, the range is extended by at least 1° in all directions, ensuring that the operational Line of Sight (LoS) is positioned within this range before operation.

Mirror M7 is flat, made of Zerodur, and coated with gold for high reflectivity at the laser wavelength. Focus adjustments at the divertor are achieved through horizontal translation of mirrors M7 and M8, which shifts the LoS and compensates for up to 75 mm in focal position. The off-axis parabolic mirrors M8 and M10 are identical, each featuring a 90° angle and concave surface, while M9 is a flat Zerodur mirror (Fig. 7).

The precision of the scanning mirror system is defined by its tilting step, which shifts the line of sight (LoS) at the divertor target. This shift must be significantly smaller than the minimum gap between the W blocks (0.5 mm poloidal), with a shift of 0.2 mm corresponding to a M7 mirror tilting angle of about 0.0008° The FSMU mirror box can also rotate around the M10 mirror's optical axis to adjust for the horizontal thermal displacement of the port plug.

3.2.2. Ex-vessel optics in the bioshield

In the bioshield (Fig. 3a), a cold dogleg, consisting of two flat mirrors (M11 and M12), is positioned to reduce neutron penetration into the port cell. The alignment of the axis for the ex-vessel optics with the axis of the port plug optics is achieved through the combined movement of the FSMU (tilting of the FSMU boxes and translation of M8) and the dogleg optics. Each mirror in the dogleg is equipped with a hexapod stage for remote 6 degree of freedom adjustments.

3.2.3. Ex-vessel optics in the PCSS

In the port cell, the optics combine the laser beam path with the observation path, incorporating VIS and NIR cameras, light collection optics for pyrometers, and a laser beam collimator. The VIS camera operates within a wavelength range of 600 nm to 900 nm. It offers a maximum field of view of 98 × 98 mm^2 at the divertor if a rectangular image sensor having diagonal size of 1.5 inch is used. The image quality of this camera remains close to the diffraction limit, ensuring an imaging resolution of about 0.1 mm at the divertor surface.

The NIR camera covers a wavelength range from 2.1 μm to 2.3 μm, providing a field of view of 12 × 12 mm^2 at the divertor. This camera is optimized for capturing infrared thermal emission with a frame rate of up to 9.6 kHz for 192 × 192 pixels windowing (FLIR X6980 high-speed MWIR camera, Teledyne FLIR LLC), which is vital for monitoring thermal distribution in the target region.

Radiometric calibration will utilize a Black Body source placed at Intermediate Focus Image 1 (see Fig. 3b), with temperatures ranging

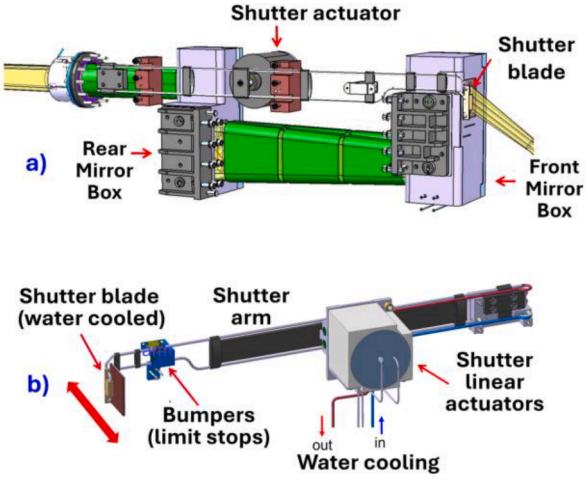

Fig. 6. a) Layout of the boxes with attached mirrors and shutter, b) Shutter assembly.

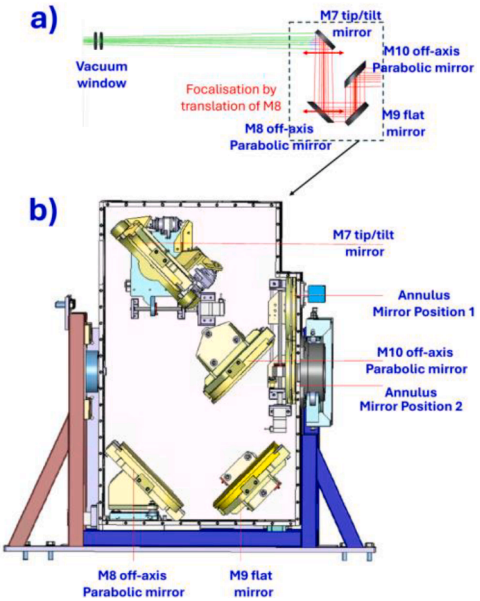

Fig. 7. Fast scanning mirror unit a) optical design and b) the mechanical layout.

from 400 °C to 1000 °C. This calibration, combined with transmittance monitoring of the optical system, will ensure absolute calibration of the detectors and evaluate any degradation.

3.2.4. *Ex-vessel components in the T-Building*

The Tritium building contains the high-power laser and pyrometers designed for temperature measurement at the laser hot spot on the divertor baffle. The laser transmits light through an optical fibre approximately 30 m long to the PCSS area, while the pyrometers have their own separate optical fibres of the same length for accurate light collection. The pyrometer system includes three high-speed infrared pyrometers (Pyroskop 840) with a 10 µs time resolution, operating in the 1.4 µm to 2 µm wavelength range, each targeting specific sub-ranges: 1.4 - 1.6 µm, 1.6 - 1.8 µm, and 1.8 - 2.0 µm. An optical setup in the T-Building splits light between the pyrometers and connects to the Port Cell optical system using a 400 µm fibre, resulting in a 3 mm spot size at the laser irradiation area.

The laser under consideration is a YLS-Series High Power Ytterbium Fibre Laser from IPG Photonics, operating at a wavelength of 1070 nm, with a maximum power output of 60 kW in continuous or pulsed mode, allowing laser pulse durations of 1 to 3 ms. It requires a high-capacity electrical supply in the T-Building, operating at 400–480 V and 50–60 Hz, with power consumption ranging from 154 kW to 174 kW.

4. Required laser output power and mirror materials

As discussed in Section 2, a power density of approximately 665 MW/m^2 is required for a 1 ms pulse duration to desorb the entire content of hydrogen isotopes from a deposited layer of 100 µm. For the selected laser spot size of 5 mm in diameter, a laser power of about 60 kW is required, assuming a reflectivity of 50% of the laser power on the divertor surface and a total optical transmission of 44%.

Fig. 8 illustrates the laser operating parameter space in terms of mirror reflectivity. In this study, 15 mirrors (with spectral reflectivity $R \geq 94\%$) and 1 double vacuum window in the laser beam line were considered. The mirror surfaces are assumed to be made of annealed copper. Two operating cases are considered, with pulse durations of 1 ms and 3 ms. The upper boundaries of the operating spaces (in red) are defined by the power density at which the divertor material, in this case tungsten, would start to melt during the laser irradiation. The lower boundaries (in blue) define the absolute minimum power density at which the entire content of hydrogen isotopes will be desorbed during a single laser pulse. The left (green) curve represents the maximum power density at which plastic deformation of the mirror substrate occurs. This curve was obtained using the threshold temperature increase for plastic deformation of annealed copper, estimated to be approximately 11.3 °C. This value was calculated using Eq. (4) from Ref. [25], taking into account that plastic deformation occurs when the transverse stress exceeds the yield strength. Based on this threshold, the maximum allowable power density was calculated. The selected laser's maximum power of 60 kW remains well within this safe operating range for the laser pulse duration of 1 ms, as can be seen in Fig. 8. For laser operation with a pulse duration of 3 ms, the maximum available power is more than sufficient and must be adjusted (reduced) to remain within the allowable operating parameter space. At the same time, it is evident that only mirrors with higher surface spectral reflectivity can be used. The suitable materials for the LID laser with a wavelength of $\lambda = 1.064$ µm are Au ($R \approx 99\%$), Ag ($R \approx 98.5\%$), Cu ($R \approx 97\%$), and Al ($R \approx 96.5\%$) [26]. However, Ag and Al can activate into very long-lived isotopes, making the use of these materials problematic. Therefore, Au and Cu are the best alternatives.

Gold and copper were selected in our project as coatings for all metallic mirrors in the beam path due to their excellent and consistent reflectivity in the infrared wavelength range. These coatings also provide very good reflectivity in the visible range down to approximately 550 nm, enabling optimized reflection of the high-power laser (~97–99%) and sufficient reflectivity for the pilot laser and returned visual image. The pilot laser used for visualizing the main laser spot location on the divertor tiles will operate at a wavelength of approximately 660 nm.

5. Summary

The paper discusses the challenges associated with tritium inventory management in ITER and future fusion devices, emphasizing the need for accurate determination of tritium amounts and their spatial distribution within the vacuum vessel. As a licensed nuclear facility, ITER is required to limit tritium retention to a maximum of 1 kg in the vacuum vessel, with specific limits on tritium trapped in divertor cryopumps and measurement uncertainties.

To address this, a laser-based T-monitor diagnostic system has been proposed by Forschungszentrum Jülich, which utilizes Laser-Induced Desorption and Residual Gas Analysis to measure tritium concentrations on the inner divertor tiles. This diagnostic method, proven effective in other fusion devices, offers precise and spatially resolved maps of fuel retention, enabling assessments of detritiation methods.

The paper presents the optical design of the T-monitor, incorporating a high-power laser and durable metallic mirrors to transport laser beams in the near-infrared spectrum while allowing for coaxial observation in the visible range. Key requirements include measuring hydrogen isotope

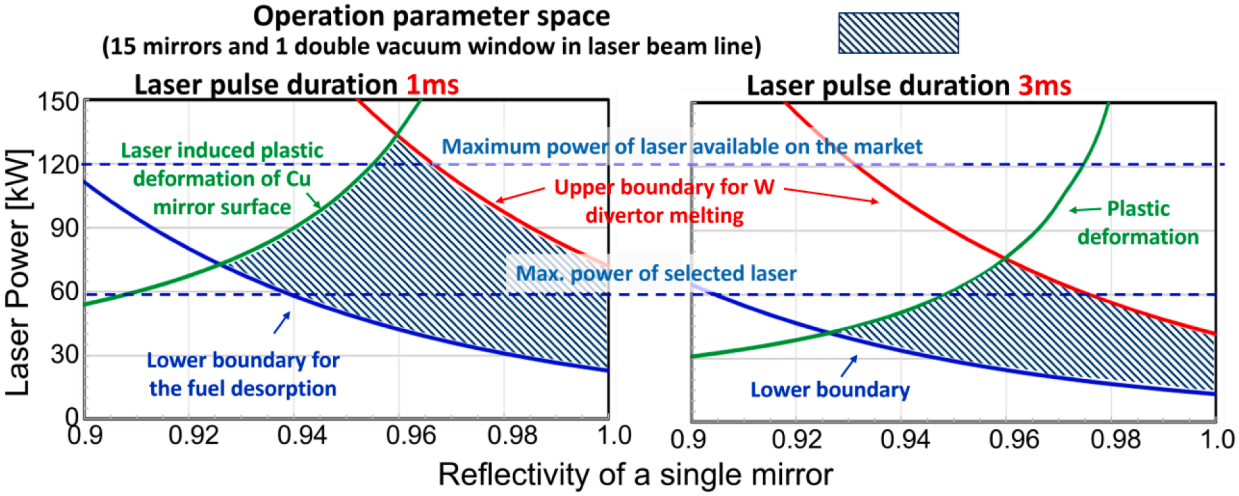

Fig. 8. The operating parameter space in terms of laser power and the reflectivity of a single mirror.

concentrations in specific areas of the divertor, with detailed specifications for the scanning area, laser parameters, and expected tritium concentrations.

The LID-QMS diagnostic involves heating designated areas of the wall to 1600 K using laser pulses, allowing for the desorption of hydrogen isotopes. Measurements must maintain a relative accuracy of 20%, with specific spatial resolution requirements detailed for the laser spot size and pulse duration.

The optical system includes various components for in-vessel and ex-vessel optics, such as mirrors, a shutter, and cameras designed for visible and infrared wavelengths. A Fast Scanning Mirror Unit is incorporated for precise laser positioning on the divertor baffle, enabling rapid adjustments of the optical diagnostic setup.

The paper concludes with a discussion on required laser output power and mirror materials. A pneumatic shutter system is introduced for protecting optical elements from contamination, while also allowing for the monitoring of the optical transmittance.

CRediT authorship contribution statement

A. Huber: Supervision, Formal analysis, Writing – original draft, Project administration. **Ph. Andrew:** Project administration. **G. Sergienko:** Investigation, Formal analysis. **J. Assmann:** Validation. **D. Castano:** Formal analysis. **A. De Schepper:** Project administration, Funding acquisition. **S. Friese:** Formal analysis. **I. Ivashov:** Formal analysis, Software. **D. Kampf:** Formal analysis, Investigation. **Y. Krasikov:** Methodology, Conceptualization, Supervision, Formal analysis. **H.T. Lambertz:** Visualization. **Ph. Mertens:** Investigation, Formal analysis. **K. Mlynczak:** Investigation, Formal analysis. **K. Rasinska:** Resources. **M. Schrader:** Investigation, Conceptualization, Formal analysis. **D. Van Staden:** Validation, Formal analysis. **A. Terra:** Formal analysis. **Xi Jiang:** Formal analysis, Project administration. **M. Zlobinski:** Formal analysis. **A. Reutlinger:** Project administration. **S. Brezinsek:** Project administration. **Ch. Linsmeier:** Project administration.

Declaration of competing interest

The authors declare that they have no known competing financial interests or personal relationships that could have appeared to influence the work reported in this paper.

Acknowledgments

This work is supported by the ITER Organization under the Cooperation Agreement between Forschungszentrum Jülich GmbH and ITER (ref. IO/21/CT/4300002506). The views expressed do not necessarily reflect those of the ITER Organization.

Data availability

Data will be made available on request.

References

[1] G. De Temmerman, et al., Efficiency of thermal outgassing for tritium retention measurement and removal in ITER, Nucl. Mater. Energy 12 (2017) 267–272.
[2] R.A. Pitts, et al., Plasma-wall interaction impact of the ITER re-baseline, Nucl. Mater. Energy 42 (2025) 101854.
[3] M. Zlobinski, et al., Laser-Induced Desorption of co-deposited Deuterium in Beryllium Layers on Tungsten,, Nucl. Mater. Energy 19 (2019) 503–509.
[4] A. Huber, et al., In-situ measurement of trapped hydrogen by laser desorption in TEXTOR-94, Phys. Scr. T94 (2001) 102–105, https://doi.org/10.1238/Physica.Topical.094a00102.
[5] B. Schweer, et al., In situ detection of hydrogen retention in TEXTOR by laser induced desorption, J. Nucl. Mater. 390–391 (2009) 576–580.
[6] M. Zlobinski, et al., First results of laser-induced desorption - quadrupole mass spectrometry (LID-QMS) at JET, Nucl, Fusion 64 (2024) 086031.
[7] S. Carpentier, et al., Modelling of beryllium erosion–redeposition on ITER first wall panels, J. Nucl. Mater. 415 (2011) S165.
[8] K. Schmid, et al., WALLDYN simulations of global impurity migration in JET and extrapolations to ITER, Nucl. Fusion 55 (2015) 053015.
[9] K. Schmid, et al., Full WITER: Assessment of expected Werosion and implications of boronization on fuel retention, Nucl. Mater. Energy 41 (2024) 101789.
[10] A. Loarte, et al., The new ITER baseline, research plan and open R&D issues, Plasma Phys. Control. Fusion 67 (2025) 065023.
[11] C.C. Klepper, et al., Developments and challenges in the Design of the ITER DRGA, IEEE Trans, Plasma Sci. 50 (2022) 4970–4979.
[12] T. Hirai, et al., Use of tungsten material for the ITER divertor, Nucl. Mater. Energy 9 (2016) 616–622, https://doi.org/10.1016/j.nme.2016.07.003.
[13] J.H. Yu, et al., Deuterium desorption from tungsten using laser heating, Nucl. Mater. Energy 12 (2017) 749–754.
[14] R. Villari, et al., Nuclear analysis of the ITER full-tungsten divertor, Fusion Eng. Des. 88 (2013) 2006–2010.
[15] T. Schwarz-Selinger, et al., A critical review of experiments on deuterium retention in displacement-damaged tungsten as function of damaging dose, Mater. Res. Express 10 (2023) 102002.
[16] O.V. Ogorodnikova, V. Gann, Simulation of neutron-induced damage in tungsten by irradiation with energetic self-ions, J. Nucl. Mater. 460 (2015) 60–71.
[17] Sub-system requirement document sSRD-55.GC: tritium monitor 2025 https://user.iter.org/?uid=WYWX2X.
[18] J. Romazanov, et al., Validation of the ERO2.0 code using W7-X and JET experiments and predictions for ITER operation, Nucl. Fusion 64 (2024) 086016, https://doi.org/10.1088/1741-4326/ad5368.
[19] K. Schmid, T. Wauters, W ITER Full, Assessment of expected Werosion and implications of boronization on fuel retention, Nucl. Mater. Energy 41 (2024) 101789.
[20] J. Roth, et al., Tritium inventory in ITER plasma-facing materials and tritium removal procedures, Plasma Phys. Control. Fusion 50 (2008) 10300, https://doi.org/10.1088/0741-3335/50/10/103001.
[21] A. Burdakov, et al., Integration of Iter Diagnostics Ports in binp, Fusion Eng. Des. 178 (2022) 113114.
[22] Ansys Zemax OpticStudio, 2025 https://www.ansys.com/products/optics/ansys-zemax-opticstudio.
[23] I. Ivashov et al.I. Ivashov et al. , Optical System Development Challenges in ITER T-Monitor Diagnostic, these proceedings 2025.
[24] S. Friese, Integration of a laser-based calibration source into the protection shutter for the ITER T-monitor diagnostic, these proceedings 2025.
[25] J.P. Blanchard, Practical considerations for thermal stresses induced by surface heating, Fusion Sci. Technol. 44 (1) (2003) 101–105, https://doi.org/10.13182/FST03-A317.
[26] https://refractiveindex.info/ 2025.